Korean J. Chem. Eng., 39(5), 1350-1360 (2022)
DOI: 10.1007/s11814-021-1038-3

pISSN: 0256-1115
eISSN: 1975-7220

Oxidized gum arabic cross-linked pectin/O-carboxymethyl chitosan: An antibiotic adsorbent hydrogel

Reza Darvishi*,†, Hajar Moghadas*, and Ali Moshkriz**

*Department of Gas and Petroleum, Yasouj University, Gachsaran, 75918-74831, Iran
**Department of Chemical Engineering, Faculty of Engineering, Arak University, Arak, 38156-8-8349, Iran
(*Received 28 June 2021 • Revised 13 November 2021 • Accepted 10 December 2021*)

Abstract−The current work investigated the synthesis possibility of oxidized gum arabic cross-linked pectin/O-carboxymethyl chitosan hydrogels (OGA-Pc-O-CMCS) as a pH-sensitive adsorbent vehicle. During the hydrogel fabrication, the cross-linker oxidized gum arabic (OGA) plays an important role in the enhancement of mechanical stability and the structural compactness of the hydrogel. The effect of OGA content, reaction time, reaction temperature, and reaction pH on the hydrogel swelling and crosslink degree was evaluated, modeled, and optimized statistically using response surface methodology (RSM) based on central composite design (CCD). As the pH of pectin/O-Carboxymethyl chitosan (Pc-O-CMCS) complexation increased up to 6.0, the swelling degree of the hydrogels decreased regardless of the concentration of the OGA. The swelling indices of 101.35% and 70.552% showed the optimum RSM results in the acidic and neutral medium, respectively. The adsorption efficiency of two conventional fluoroquinolones antibiotics (Levofloxacin (LVX) and Delafloxacin (DLX)) in the optimized hydrogel formulations was investigated. The obtained results confirmed that OGA concentration was an important parameter in the swelling processes. The adsorption capacity of the hydrogels was higher in acidic medium (pH 3.9) compared to natural medium (pH 7.1), which indicates the pH-sensitive adsorption behavior of the prepared hydrogel. The maximum antibiotic adsorption occurred after 12 hours: (66.3-87.5%) and (45-53%) for pH 3.9 and 7.1, respectively. The shape and morphological analysis of the beads before and after adsorption was performed using field emission scanning electron microscopy (FE-SEM). The FE-SEM analysis revealed that the shape of the beads changed significantly because of erosion and swelling activity after antibiotics adsorption. Experimental results exhibited that SIP model fitted best to the isotherm adsorption of LVX and DLX onto OGA-Pc-O-CMCS hydrogel.

Keywords: Hydrogel, Oxidized Gum Arabic, Fluoroquinolones (FQs) Antibiotic Adsorption, Pectin-O-Carboxymethyl Chitosan, Response Surface Methodology (RSM), Swelling Index

INTRODUCTION

Drugs discharged in the aquatic environment are a serious problem that threatens earth and human life. The potential risks of the drug with bio-active compounds are greater than the others [1]. Antibiotics are highly bioactive compounds that are frequently used and widespread in the environment and aquatic ecosystems [2]. For example, the existence of fluoroquinolones as commonly used antibiotics is widely reported in wastewaters and water reservoirs, such as drinking, surface, ground, and ocean water [3].

Detecting antibiotics in different water reservoirs demonstrates the importance of their removal from the water by developing effective techniques [4]. To date, various methods have been reported for antibiotics removal from water including biodegradation [5], electrochemical oxidation [6], advanced oxidation [7], photo catalytic [8], and adsorption [9]. Among them, the adsorption method is more popular and widely used because it is easily performed. In adsorption methods, different adsorbents are used, such as minerals [10], carbon nanomaterials [11], polymer hydrogels [12], and composite materials [13].

In contaminated water absorption, non-toxic biocompatible and bio-degradable absorbents are preferred [14]. For that purpose, natural polymers such as hydrogels are good candidates [15]. Swelling hydrogels dispersed into the water is disadvantageous and makes some difficulty for separating the hydrogel particles from the water [16]. By cross-linking the hydrogel, a bulk body is produced instead of dispersing particles [17]. One of the extensively used agents for potential cross-linking the proteins and amino group-containing polymer in the preparation of hydrogels is OGA [18]. Actually, GA is a complicated variable mixture of arabinogalactan, glycoproteins, oligosaccharides, and polysaccharides that is non-toxic and biodegradable [19]. OGA is oxidized with periodate and produces aldehyde groups by the cleavage of diols present in the sugar units [20]. For antibiotic adsorption, a multi-component polymer system needs to be designed and optimized for suitable performance [21]. In the present work, a multi-component hydrogel (Pectin/O-Carboxymethyl chitosan and oxidized gum arabic) was designed, formulated, manufactured and optimized for fluoroquinolone antibiotics adsorption such as Levofloxacin (LVX) and Delafloxacin (DLX). With respect to the maximum hydrogel swelling and cross-linked degree, first the amount of AG, the interaction medium pH and temperature, and reaction time were optimized. Then the absorption effi-

†To whom correspondence should be addressed.
E-mail: r.darvishi@yu.ac.ir

ciency of the optimized hydrogel was evaluated for Lev and Del antibiotics. The hydrogel was produced in a bead form. The effect of independent variables on the hydrogel bead swelling and crosslink degree was statistically evaluated via response surface methodology (RSM) using central composite design (CCD). The antibiotic absorption efficiency of the hydrogel beads was measured using reversed-phase HPLC (RP-HPLC). The adsorption isotherm and kinetics were also done on the samples. The shape and morphological feature of the beads was investigated by SEM before and after antibiotic adsorption.

EXPERIMENTAL SECTION

1. Materials

Pectin was purchased from Merck Co, silver nitrate, sodium periodate, acetic acid, trimethylamine, buffer phosphate, ninhydrin, isopropanol, glycine gum arabic and glycine were supplied by Sigma Aldrich. Levofloxacin (LVX), 98% Delafloxacin (DLX) were supplied by Tehran Darou.

2. Preparation of OGA

The oxidation method was similar to that described in earlier work [22]. For 10% oxidation, 10 g (0.058 mol) of GA was dissolved in 80 mL distilled water, and 1.24 g of sodium periodate was dissolved in 20 mL water. The sodium periodate solution was mixed with GA solution and then stirred for six hours at room temperature in dark. For periodate removal, a dialysis tube of MWCO 6000-8000 was employed for three days against distilled water. Purification was checked by adding 1 mL of silver nitrate solution (1%) to 1 mL of the dialysate. The purified dialysate was then frozen and lyophilized.

3. Preparation of OGA Cross-linked P/O-CMCS Beads

O-CMC with a degree of substitution of 0.35 was made similar to reference [23]. OGA cross-linked P/O-CMCS beads were formulated using the experimental design presented in Table 1. The beads were prepared according to a general method with some modification [24-26]. The ratio of pectin and O-CMCS was 1 : 1, and kept constant in all experiments. Pectin and OGA were separately dissolved in distilled water (10 ml) and stirred at 30 °C to obtain homogeneous solutions. O-CMCS powder was dissolved in 10 ml of 2% acetic acid and stirred at 25 °C. The solutions of pectin and O-CMCS were carefully mixed, and then OGA solution was added while the mixture was stirred until the beads were produced. Continuous stirring improved the bead mechanical strength and prevented the accumulation of material. The beads were filtered and then washed with hot and cold water followed by vacuum drying at 35 °C. Dried samples were wrapped in aluminum foil and stored in a desiccator for further use.

Table 1. Relationship between the coded and real variables for RSM

Variables	Codes	Units	Levels				
			$-\alpha$	−1	0	1	$+\alpha$
Time	X_1	min	5	10	15	20	25
pH	X_2	-	1	3	5	7	9
Temperature	X_3	°C	50	60	70	80	90
OGA	X_4	%	5	15	25	35	45

4. Infrared Study

Interactions between the components were investigated via Fourier transform-infrared (FTIR) spectrophotometer supported by (Thermo Scientific) NICOLET iS10, from 600 to 4,000 cm^{-1} at a resolution of 4 cm^{-1}.

5. SEM

The morphological characterization of the optimized hydrogel beads before and after antibiotics adsorption was visualized using SEM type (LVEM5 Benchtop Electron Microscope) as shown in Fig. 9 and Fig. 10, respectively.

6. Swelling Study

The dynamic swelling study was carried out for the prepared beads by mass measurement in different pH value of phosphate buffer solutions (pH 7.1 and 3.9). The swelling degree was measured gravimetrically by weight of the sample before and after swelling, and computed as follows:

$$\%S_w = \frac{W_t - W_o}{W_o} \times 100 \quad (1)$$

where S_w is the swelling index, W_t and W_o are the weight of the swollen beads at time t and the weight of the dry beads, respectively. The swelling indices were obtained after 24 hours.

7. Design of Experiment

Response surface methodology (RSM), a series of mathematical/statistical techniques, uses experimental data to find regression model equations and operating conditions [27]. Central composite design (CCD) is the most commonly used fractional factorial design used in the response surface model for building a second order (quadratic) model for the response variable without needing to use a complete three-level factorial experiment. Analysis of variance (ANOVA) is a conceptually simple, powerful, and popular way to analyze the differences among three or more population means.

The effect of material compositions on the swelling and crosslink degree was investigated with the aid of the design of experiments (DOE) technique. CCD was employed in which the input parameters were the effective factors (reaction time, reaction temperature, reaction pH, and OGA concentration). Four levels were assigned for the input parameters that are listed in Table 1.

RSM computations were performed by Design-Expert software (ver. 12.0). Twenty random experiments were proposed for six replicates in the mid-points. The mathematical empirical model was defined as:

$$Y = \beta_0 + \sum_{i=1}^{n} \beta_i x_i + \sum_{i=1}^{n-1} \sum_{j=i+1}^{n} \beta_{ij} x_i x_j + \sum_{i=1}^{n} \beta_{ii} x_i^2 + \varepsilon \quad (2)$$

where Y is the response or dependent variable (Y_1=Swelling Ratio and Y_2=Crosslink Degree). X_i and X_j represent the independent variables (X_1=reaction time, X_2=reaction pH, X_3=reaction temperature and X_4=OGA content). i and j are the indices; β_0, β_i, β_{ii}, β_{ij} are the coefficients of the regression; and ε represents the random error. Significant differences between the independent variables ($p<0.05$) were determined by analysis of variance (ANOVA).

8. Crosslink Degree Determination

The crosslinking degree was determined based on the amino groups [28]. Dried hydrogel of 8 mg was placed in the mixture of

deionized water (8 mL) and ninhydrin solution (4 mL) and warmed at 100 °C for up to 20 min. Afterward, the sample was cooled to room temperature, and then 20 mL 50% isopropanol was added to the mixture. A spectrophotometer at 570 nm was used to estimate the absorbance. The concentration of free amino groups was obtained using a standard curve of glycine concentration versus absorbance. The crosslinking degree was calculated as below:

$$\text{Crosslink degree} = \frac{M_0 - M_t}{M_0} \times 100 \quad (3)$$

where, M_0 and M_t was the mole fraction of free amino groups in uncross linked and cross linked sample, respectively.

9. Adsorption Study

Different weights (0.5-5 g/L) of optimized hydrogel sample (OHS) were added to a group of 250 mL flasks with 100 mL of the VLX and DLX solutions of various initial concentration (25-225 ppm) at different pH (1-11). The flasks were shaken with a speed of 200 rpm at different temperatures (25-55) for different time intervals. The amount of VLX and DLX adsorption was determined using an RP-HPLC (HPLC, ECIL, 4100) equipped with UV/V (mode 14200) and C18 column (250 mm×4.6 mm, 5 μm). The flow rate was adjusted to 1 mL/min, the wavelength was set at 320 nm for the volume injection of 500 μL. Mobile phase (Methanol/Buffer 40/60; Buffer 25 mM phosphate and 15%v/v triethylamine) with flow rate 1 ml/min was applied. Each adsorption experiment was performed three times and the data were averaged.

RESULTS AND DISCUSSION

1. Design of Experiment

The behavior of the crosslink reaction and swelling indices was investigated by considering the effect of four reaction parameters, including the reaction time, temperature, pH, and the concentration of OGA applying the CCD-RSM method. The experimental results of the impact of the reaction parameters on swelling and crosslink degree of the prepared hydrogels at neutral medium (7.1) are shown in Fig. 2. To investigate the effect of each component on the hydrogel characterization, the DOE technique was employed. The input variables of a CCD were chosen as reaction time (min), temperature (°C) and pH, and the amount of OGA (%) to study their impact on the swelling and crosslink degree of the prepared hydrogel. The hydrogel was fabricated using the compositions suggested by the DOE matrix that are shown in supplementary file (Table S1) along with the experimental results. The relation between the hydrogel content and the material compositions was as follows:

$$\begin{aligned} Y_1 = {} & +80.03 - 16.51X_1 - 14.41X_2 - 10.23X_3 - 10.05X_4 \\ & + 0.0250X_1X_2 - 1.66X_1X_3 - 0.0250X_1X_4 + 0.4\,X_2X_3 - 1.84\,X_2X_4 \\ & - 0.9\,X_3X_4 + 3.01X_1^2 + 8.47X_2^2 - 1.31X_3^2 + 6.93X_4^2 \end{aligned} \quad (4)$$

$$\begin{aligned} Y_2 = {} & 76.60 + 7.48X_1 + 8.20X_2 + 8.69X_3 - 4.05X_4 + 0.0063X_1X_2 \\ & + 0.4563X_1X_3 - 0.0063X_1X_4 - 0.0063X_2X_3 + 0.3562X_2X_4 \\ & - 0.0562X_3X_4 - 1.17X_1^2 - 5.33X_2^2 + 1.39X_3^2 - 5.61X_4^2 \end{aligned} \quad (5)$$

where, Y_1 and Y_2 are the swelling and crosslink degree, respectively. X_1, X_2, X_3, and X_4 represent the time, PH, temperature, and OGA content, respectively. The ANOVA data of the quadratic models were listed in supplementary file (Table S2). As can be seen, the F-value for Y_1 and Y_2 was equal to 676.83 and 1,410.19, respectively. Both models suggest a very low p-value (<0.00001), which confirmed the high significance of the models for data approximation. The R^2 values for Y_1 and Y_2 were 0.9984 and 0.9992, respectively, which confirmed good agreement between the experimental and the estimated data by the models. Dada in supplementary file (Fig. S1) demonstrate that the significant interaction between the input variables was X_1X_3 (time and PH), X_2X_4 (Temperature and OGA) and also X_3X_4 (PH and OGA).

Fig. 2(a) and (d) show the variation of the swelling indices and crosslink degree of the hydrogels based on PH and time variation, respectively. Swelling indices decreased with the increasing of the pH of the reaction medium up to neutral pH (~7). After that, a further increase in pH led to a decrease swelling index. The obtained data confirm that the swelling process of the prepared beads was pH-sensitive. The swelling behavior of the beads in a neutral medium can be related to the high hydrophilicity of the hydrogel chains (-OH, -COOH, and NH2- polar groups of the OGA, Pectin, and O-CMCS, respectively). In neutral pH, water tends to diffuse into the hydrogel chains to make a hydrogen bond with the -OH, -COOH, and NH2- groups. Filling up the space along the chains resulted in increased swelling capacity. A reversed pattern was demonstrated for the crosslinking degree as PH varied. By increasing the reaction time, the crosslinking degree increased. Then the crosslinking degree seemed to level off at 37% without any further appreciable change. That behavior indicates that the maximum possible crosslink takes place. Over time, the reaction medium became more viscose. Higher viscosity leads to a decrease in the chain's accessibility for link together by covalent crosslink. The trend of the swelling degree is inverse. The swelling index showed a downward trend as the time reaction increased.

The structure of the pectin/O-Carboxymethyl chitosan crosslinked with oxidized gum arabic (OGA-Pc-O-CMCS) may have been obtained via the formation of covalent bonds between the hydroxy groups of the D-galacturonic acid residue present in the structure of pectin and the carbonyl group located in one end of the oxidized gum Arabic; the other free end of the oxidized gum Arabic molecule binds at two hydroxyl and amine groups present in the chain of the O-Carboxymethyl Chitosan (Fig. 1).

The effect of the OGA concentration and reaction temperature on the swelling indices and crosslink degree are illustrated in Fig. 2(b) and (e), respectively. As the reaction temperature increased, the swelling indices decreased, while the crosslinking degree increased. The variation of the swelling indices versus the OGA concentration shows a minimum while a maximum is seen in the crosslink degree profile in different OGA concentrations.

The impact of the OGA content and temperature on swelling indices and the crosslink degree is presented in Fig. 2(b) and (d), respectively. As the amount of OGA increased, the curve of the swelling indices changed concavely, whereas the crosslinking degree varied convexly. For an optimum crosslink, a balance between the number of amino groups and aldehyde groups is needed. Too high or too low amount of each moiety reduced the interactions. Increasing the OGA content led to an increase in the viscosity of the sample and consequently decreased the mobility of the chains and

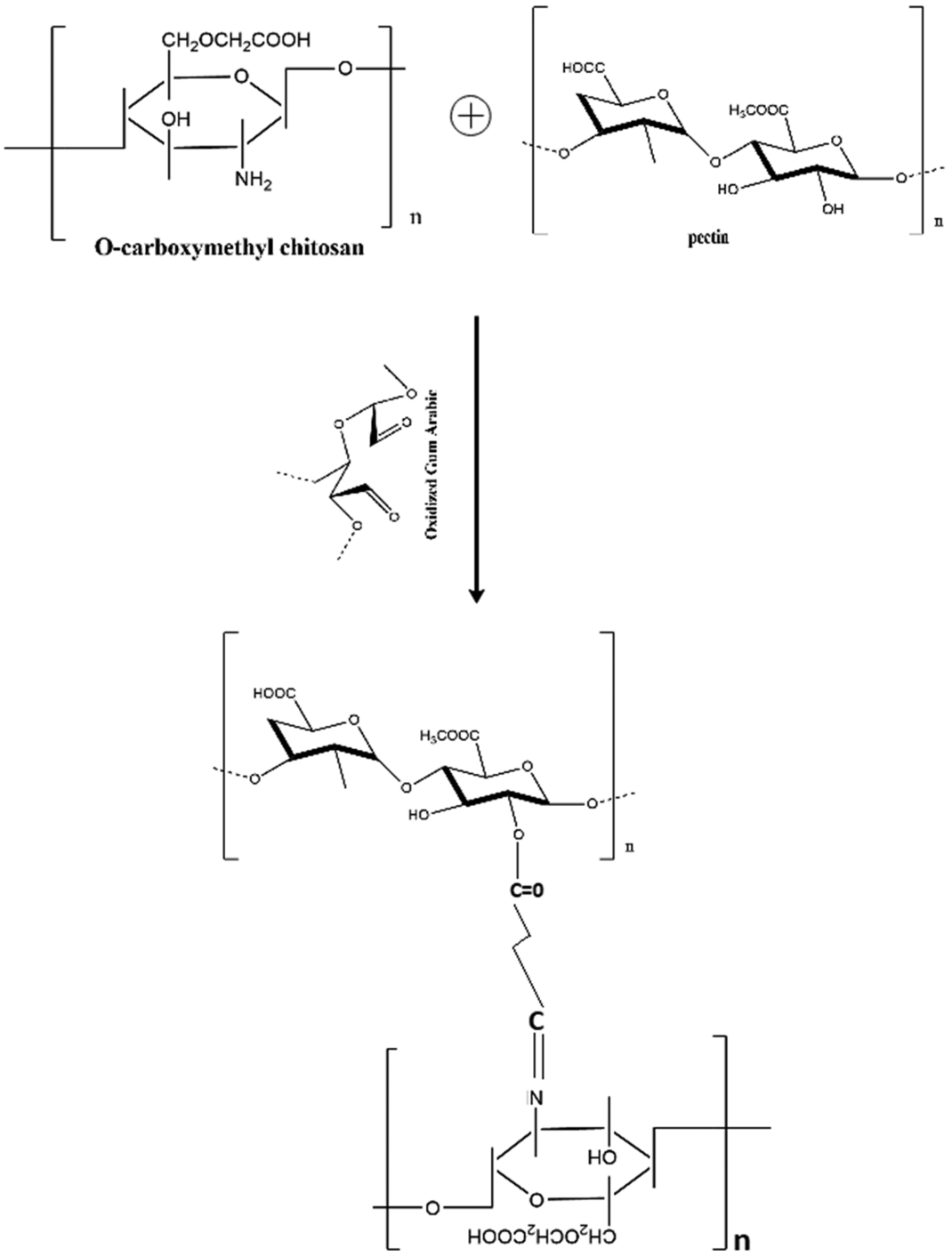

Fig. 1. Schemes of the prepared polymer components and antibiotics.

the possibility of the interaction. However, besides the viscosity, the quantity of the functional groups also impacts the crosslink process. The concave and convex behavior is demonstrated in the swelling indices and crosslink degree profiles as the PH increased, while the OGA content and the other parameters remained constant. The sensitivity to the PH can be attributed to the polyanionic nature of the pectin and OGA and the virtue amphoteric property of the OCS. In the pH range of 2-7, the crosslink reaction between aldehyde, carboxylic, and amino was increased gradually and then it was reduced steadily. In the acidic pH phase, the amino groups of O-CMCS were in the protonated form that prevented the crosslink occurrence. The isoelectric point of O-CMCS occurs within the pH range of 8-9 where the molecule does not change and phase separation happens. Before the isoelectric point, gelation takes place rapidly so the most suitable pH for the crosslink reaction is estimated as pH 6 (supplementary Fig. S1).

The profiles for obtaining the optimum values of the effective parameters and desirability function of the swelling and crosslink

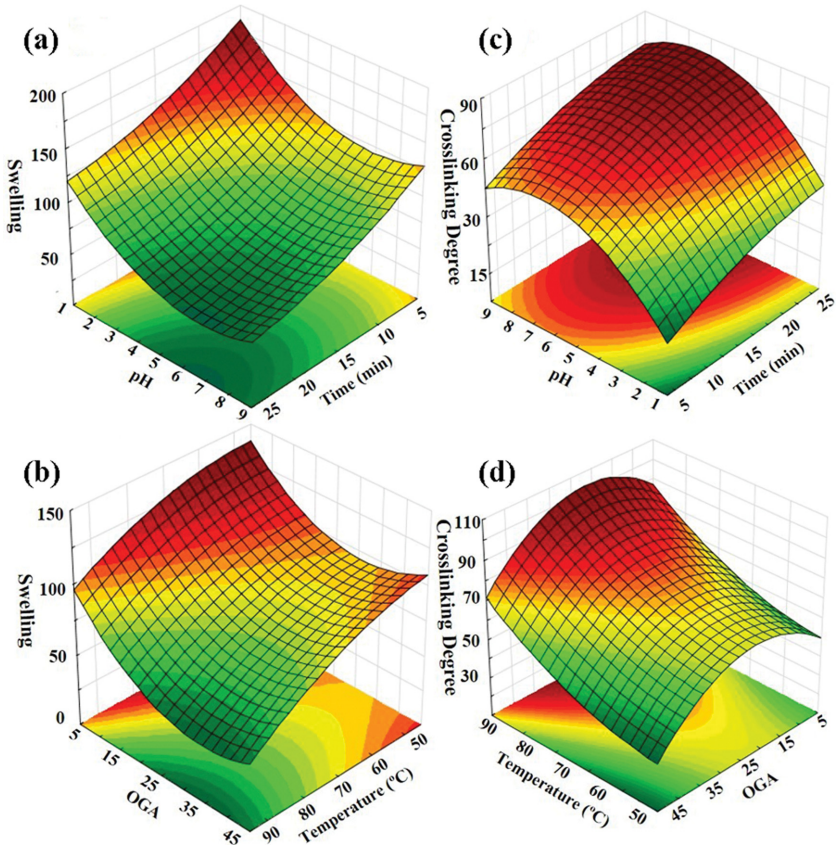

Fig. 2. Response surfaces plots at optimum conditions.

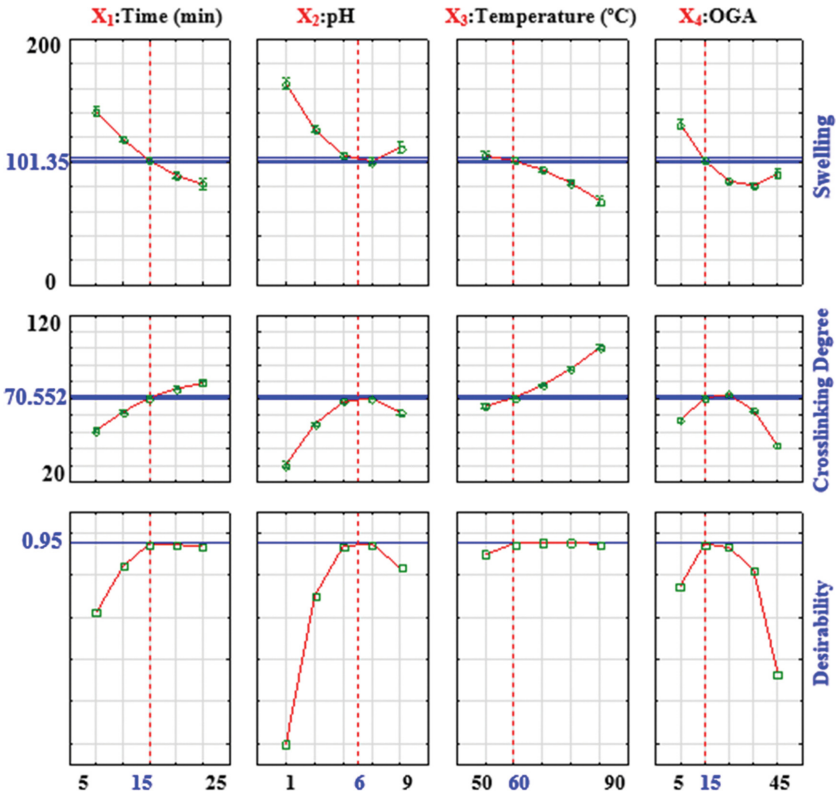

Fig. 3. Profiles for predicated values and desirability function for swelling and crosslink degree. Dashed line shows optimized parameters values.

degree are shown in Fig. 3, which indicates that optimum operational parameters values were 15 min, 6, 60 °C and 15%wt for the time, pH, temperature and OGA, respectively. At the optimum conditions, the swelling and crosslink degrees were 101.35 and 70.55, respectively, with overall desirability of 0.95.

At the optimum condition, the swelling indices of 101.35% (reaction time 15 minutes, OGA 15 wt%, 60 °C, PH 6), were predicted for the beads swelling at pH 7.1. The desirable regression coefficients of the swelling processes in a neutral medium indicated the model's ability to explain the experimental results.

2. Antibiotic Adsorption

In the next sections, the effects of different adsorption parameters such as initial VLX and DLX antibiotics concentration, temperature, prepared hydrogel dosage, solution pH, and contact time on the efficiency of the removal process are explored experimentally.

2-1. Effect of Initial Antibiotics Concentration

The experimental results of the antibiotic adsorption onto the hydrogel in neutral buffer solution pH (7.1) areshown in Fig. 4. The adsorption efficiency (q_t) and antibiotic removal (%) for different antibiotic initial concentrations are demonstrated on the left and right vertical axes, respectively. The experiment was carried out for various initial amount of antibiotic, whereas all other parameters were constant (contact time: equilibrium time, hydrogel content: 0.5 g/L and pH 7). The results indicate that the antibiotic removal of the prepared hydrogel gradually decreased while its adsorption capacity increased as the initial concentration of the DLX and LVX increased. The antibiotic removal efficiency decreased from 53.4% to 30.8% for DLX and 49.1-26.2% for LVX with an increase in the initial antibiotic content from 25 to 225 mg/L. It should be noted that because the active adsorption sites on a given mass of the adsorbent was approximately fixed; therefore when the initial antibiotic concentration in the solution increased, the quantity of the active sites on the hydrogel adsorbent was not sufficient to adsorb all antibiotic molecules and, therefore, antibiotic removal was reduced. The amount of adsorbed species onto the OGA-Pc-O-CMCS hydrogel at equilibrium, q_e (mg/g), increased with increasing antibiotic concentration at constant adsorbent dose 0.5 gL^{-1}. The experimental result shows that by increasing the initial DLX and LVX concentration from 25 to 225 mg/L, antibiotic adsorption onto the OGA-Pc-O-CMCS hydrogel adsorbent increased from 26.7 and 24.5 mg/g to 139 and 118.2 mg/g for DLX and VLX, respectively. At higher initial concentrations, an increase in concentration gradient between the antibiotic molecules in the solution and those on the hydrogel adsorbent leads to increasing the driving force of the absorption and adsorption capacity.

The data show that the removal efficiency and the adsorption capacity of OGA-Pc-O-CMCS hydrogel adsorbent for DLX were higher than LVX, which could be due to more interactions between the DLX and OGA-Pc-O-CMCS as compared to LVX and OGA-Pc-O-CMCS.

2-2. Effect of Adsorbent Dosage

The effect of adsorbent dose on the adsorption capacity and removal efficiency of prepared hydrogel adsorbent was examined in a series of adsorption experiments conducted with different adsorption dosages, varying from 0.5 to 5 g/L, while other parameters were kept constant (equilibrium time, initial antibiotic 25 mg/L, and pH 7). The results are drawn in Fig. 5. The adsorption capacity of the hydrogel adsorbent decreased from 26.7 to 3.1 mg/g for DLX and from 24.5 to 2.1 mg/g for LVX as the adsorbent doses changed from 0.5 to 5 mg/g. As can be seen from Fig. 5, the maximum removal of the DLX and LVX antibiotics was observed at 1 g/L concentration of OGA-Pc-O-CMCS Hydrogel adsorbent. This may because of the existence of higher vacant adsorption sites at this adsorbent dose. The maximum adsorption of DLX was 84.1% and for LVX it was 56%.

As the dosage of OGA-Pc-O-CMCS is increased, the value of q_t is decreasing throughout the process. This can be due to increasing in the solution viscosity, reducing accessibility to the adsorption sites, and a growth in the diffusion path length after the addition of a large amount of the hydrogel adsorbent.

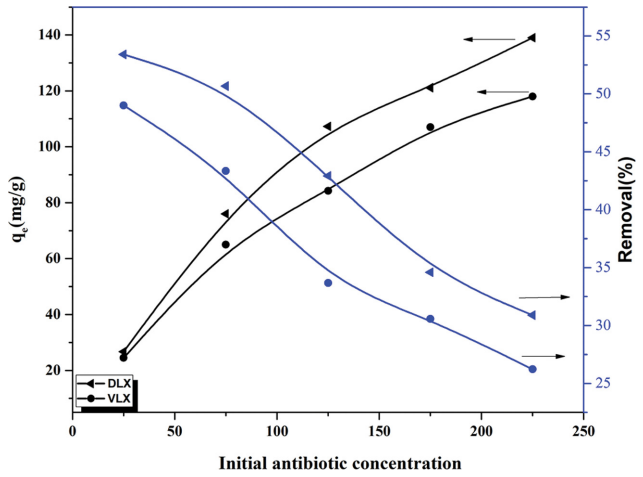

Fig. 4. The adsorption efficiency (q_t) and antibiotic removal (%) for different antibiotic initial concentrations on the left and right vertical axis. Various initial antibiotic (DLX and LVX) concentration was shown on the horizontal axes.

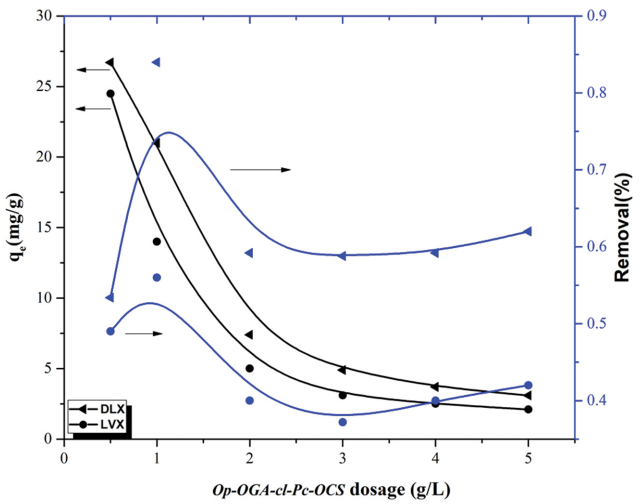

Fig. 5. Adsorption efficiency (q_t) and antibiotic removal (%) for different adsorption dosages on the left and right vertical axis. Various adsorption dosages are shown on the horizontal axes.

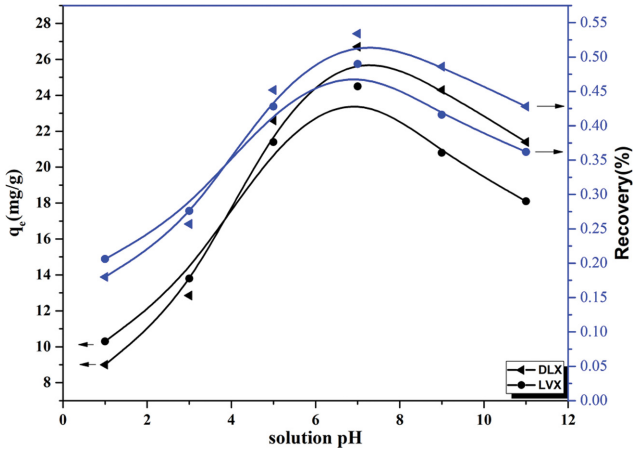

Fig. 6. Adsorption efficiency (q_t) and antibiotic removal (%) for different adsorption dosages on the left and right vertical axis. Various adsorption dosages are shown on the horizontal axes.

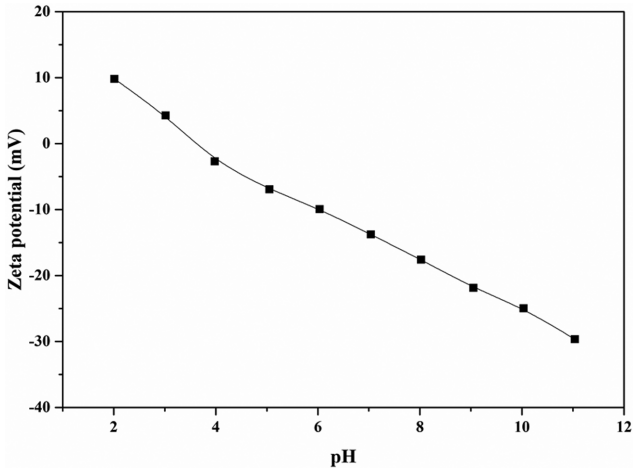

Fig. 7. Zeta-potential of OGA-Pc-O-CMCS hydrogel at different PH.

2-3. Effect of pH

The initial value of pH of the aqueous solution significantly impacts the adsorption reaction by controlling the electrostatic interaction between the materials. The effect of the solution pH on the antibiotic adsorption capacity and removal efficiency was investigated at pH 1-11 (equilibrium time, adsorbent dose: 0.5 g/L, and temperature: 303 K) in Fig. 6. As can be seen, the removal efficiency increased from 18% to 54% for DLX and from 21% to 49% as pH increased from 1 to 7. With the further increase in pH to 11, the removal efficiency decreased to 43% for DLX and 36% for LVX. Zeta-potential of OGA-Pc-O-CMCS hydrogel at different PH is given in Fig. 7. The data indicate the neutral charge of the hydrogel at pH 3-4. In the lower pH, the hydrogel became positively charged and in the higher PH, the hydrogel was negatively charged. However, the protonated amine group of the antibiotics' molecules can be adsorbed by a negatively charged hydrogel adsorbent.

Zeta-potential of OGA-Pc-O-CMCS hydrogel at different PH is shown in Fig. 7. At low acidic pH both the hydrogel and antibiotics are positively charged so the absorption is low. By increasing

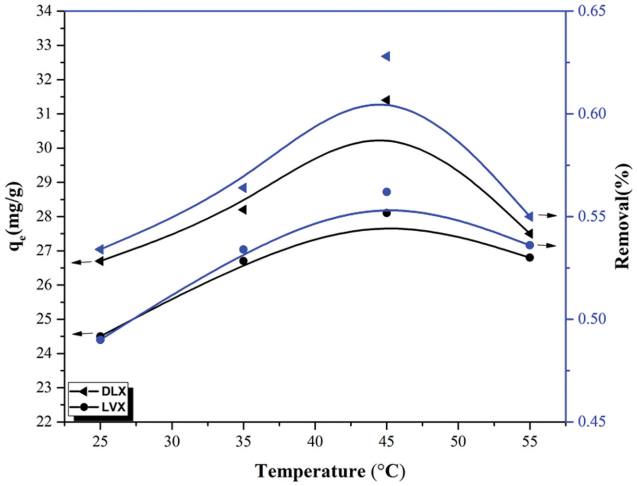

Fig. 8. Adsorption efficiency (q_t) and antibiotic removal (%) for different adsorption dosages on the left and right vertical axis. Temperature is shown on the horizontal axes.

the pH to 7, the hydrogel becomes negatively charged, which leads to an increase in the attractive force and consequently maximum adsorption. DLX and LVX are deprotonated at a neutral pH, which enhances hydrogen bond formation between polar functional groups (NH, COOH, and OH) on the hydrogel and antibiotic molecules. After that, the hydrogel becomes more negatively charged, while the antibiotics become negative at higher pH (more than pH 7) as they are in their zwitterionic form. As a result, the repulsion decreases the adsorption. The obtained data show that the hydrogel adsorbent has better removal efficiency for DLX than LVX because of the presence of a free primary amine moiety in the DLX molecule.

2-4. Effect of Temperature

The effect of temperature on the adsorption of DLX and LVX onto OGA-Pc-O-CMCS hydrogel is shown in Fig. 8. By raising temperature from 25 °C to 45 °C the rate of adsorption is enhanced, which means the process is naturally endothermic. When the temperature is increased, the matrix of OGA-Pc-O-CMCS hydrogel opens up, and the diffusion rate of the adsorbent molecule is increased. Beyond 45 °C, the rate of adsorption decreases, indicating that at a higher temperature the desorption was higher than adsorption.

2-5. Effect of Contact Time

The influence of the contact time on the DLX and LVX removal by OGA-Pc-O-CMCS hydrogel is illustrated in Fig. 9, at hydrogel dose of 0.5 g/L, initial antibiotic concentration of 25 mg/L and different time periods (2 to 120 min). The experimental data reveal that with increasing contact time both the adsorption and the removal efficiency increased and reached the maximum value after 60 min. The antibiotic removal was rapid initially and then became slow and eventually reached equilibrium. At the beginning of the adsorption process, there was a large number of vacant sites for the adsorption, so the reaction was fast. Over time, the vacant sites became occupied and, consequently, the rate of adsorption decreased. The data of the equilibrium time for different adsorbent doses from 0.5 to 5 g/L demonstrate that by increasing the adsorbent dose, the necessary time to reach the equilibrium condition

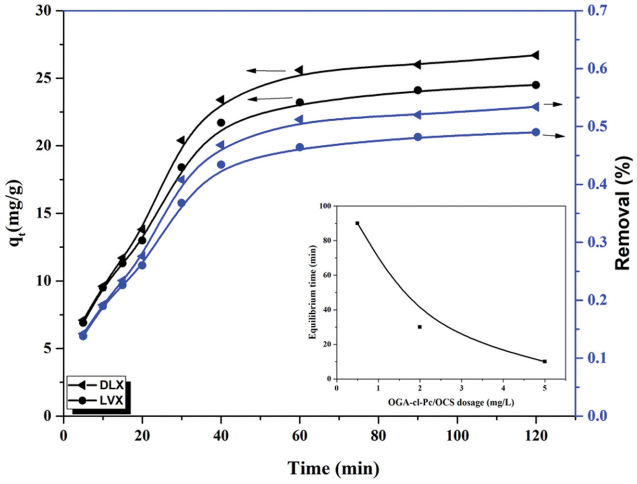

Fig. 9. The effect of contact time on the removal of DLX and LVX by OGA-Pc-O-CMCS hydrogel.

decreased, diagram inside Fig. 9.

2-6. FTIR

The chemical interactions between pectin, O-carboxymethyl chitosan, and oxidized gum arabic as the crosslinking agent and the antibiotics were investigated by the aid of FTIR spectrum (shown in Fig. 10). The spectrum of OGA-cl-Pc-O-CMCS (Fig. 10(a)) has a peak at 3,402 cm^{-1} as a result of the stretching of -OH and N-H groups. The other peaks at 2,932 cm^{-1}, 1,595 cm^{-1} and 1,078 cm^{-1} demonstrate C-H stretching vibration, N-H bending, and C-O stretching, respectively. The peaks at 1,650 cm^{-1} and 1,730 cm^{-1} were for amide and ester stretching as a result of the reaction between the aldehyde group of OGA and amine groups, and the hydroxyl group of pectin/chitosan chains. The appearance of the characteristics peaks at 3,268 cm^{-1} and 1,048 cm^{-1} (-COOH stretching), 2,848 cm^{-1}, and 1,620 cm^{-1} (alkanes -CH3 and aromatic rings, respectively), 1,725 cm^{-1} (C=O stretching vibration of the COOH group), 839 cm^{-1} (C-F peak) indicate VLX successful adsorption by the hydrogel. The appearance of the chrematistics peaks of the functional groups including -O-H stretching (3,345.89 cm^{-1}), -C-H stretching (3,075.94 cm^{-1}), ketone -C=O stretching (1,715.37 cm^{-1}), carboxylic -C=O stretching (1,623.77 cm^{-1}), C-F stretching (1,114.65 cm^{-1}) and C-Cl stretching (840.63 cm^{-1}) confirmed the DLX adsorption by the prepared hydrogel.

3. Isotherm Study

Applying the adsorption isotherms explains the mutual behavior between antibiotic content in the solution and the antibiotic quantity that was adsorbed into the adsorbent [29]. In the present study, three different adsorption isotherm models, including Langmuir, Freundlich, and SIPs models, were used to analyze the experimental data. Various fitting parameters obtained from these models are shown in Fig. 11 and Table 2. For more details about the Langmuir and Freundlich isotherms refer to [30], and the details of the SIPs model can be found in [31,32].

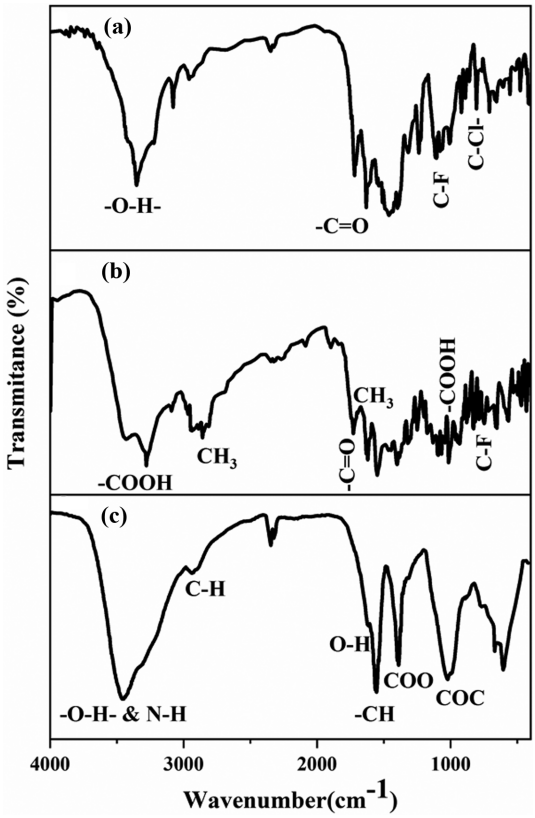

Fig. 10. FTIR spectra of (a) OGA-cl-Pc-O-CMCS, (b) OGA-cl-Pc-O-CMCS+LVX, (c) OGA-cl-Pc-O-CMCS+DLX.

For adsorption, the SIPs model presented the best fit, represented by a high correlation coefficient (R^2) of 0.999 for DLX and 0.997 for LVX compared to the other models. Maximum adsorption capacities (Qm) of DLX and LVX calculated by the SIPs isotherm model are 147.6 mg/g and 155.5 mg/g, respectively. The difference between the maximum adsorption capacities for two antibiotics was because of the difference in the nucleophilicity amount of the components. The adsorption profile matched well with the SIPs model and was also very close to the Langmuir model because of the dominant monolayer adsorption of both antibiotics onto the OGA-Pc-O-CMCS hydrogel.

4. Adsorption Kinetics and Thermodynamic Studies

The nature of adsorbate and adsorbent molecule bonding can be generalized by the aid of the adsorption kinetics [33]. For the

Table 2. Adsorption isotherm parameters obtained from Langmuir, Freundlich, and SIPs models for DLX and LVX

Sample	Langmuir			Freundlich			SIPs			
	q_l (mg/g)	K_l (L/mg)	R^2	K_f (mL/g)	1/n	R^2	Qm (mg/g)	Ks (mL/mg)	1/n	R^2
LVX	200	0.015	0.98	6.04	0.63	0.94	155.5	0.008	0.76	0.997
DLX	171	0.013	0.99	5.58	0.61	0.96	147.6	0.011	0.9	0.999

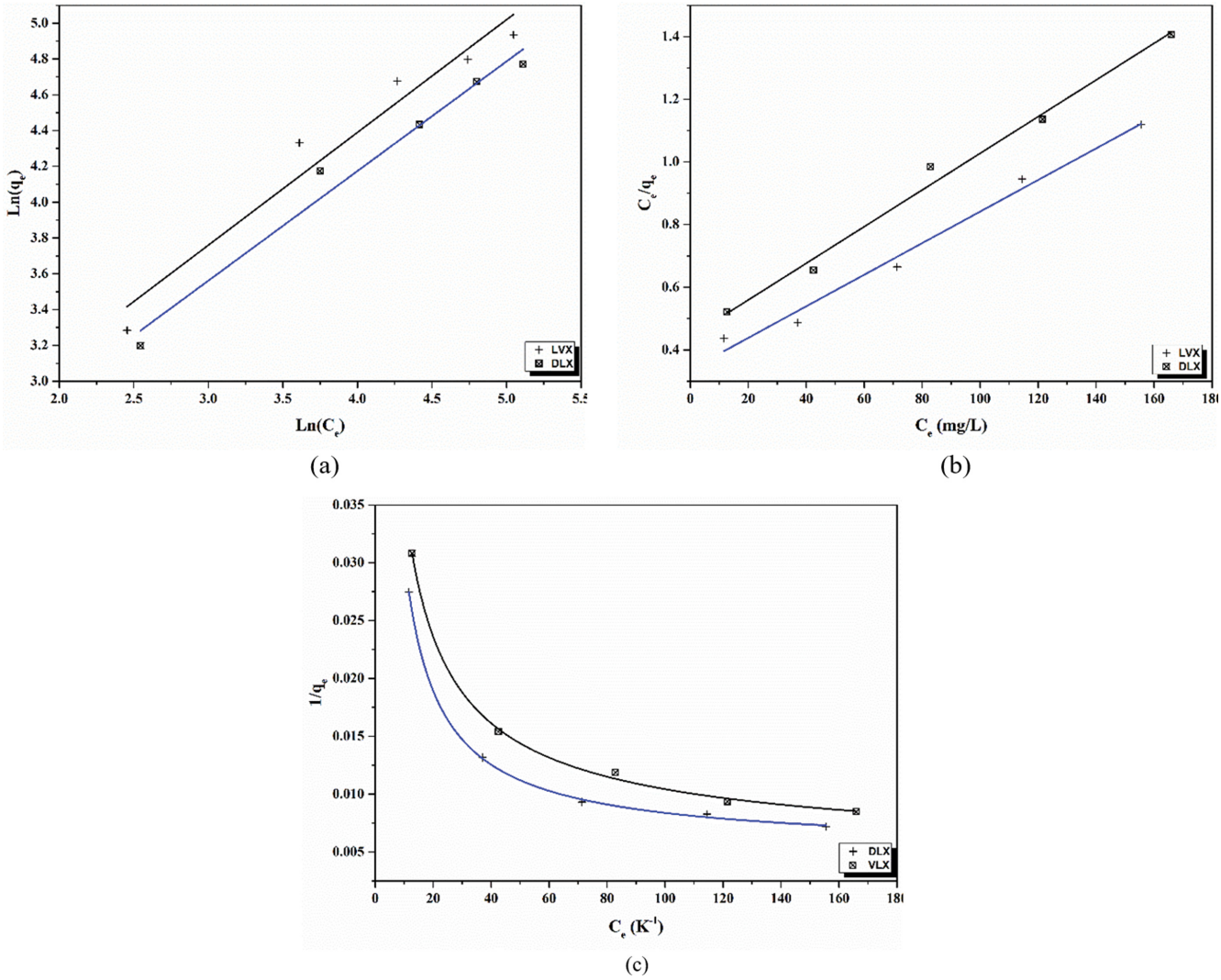

Fig. 11. Various fitting parameters obtained from (a) Langmuir model, (b) Freundlich model, and (c) SIPs model.

adsorption of DLX and LVX on the OGA-Pc-O-CMCS hydrogel, all the test conditions were set at the optimized values. The appropriate equilibrium time was approximately within 120 min for both antibiotics. The complete adsorption kinetics was investigated using two models of pseudo-first-order and pseudo-second-order kinetic models. The constant parameters and correlation coefficient of both models are demonstrated in Fig. 12 and listed in Table 3. These data show that the kinetics involved in the DLX and LVX adsorption represents cooperative adsorption. The reason can be discussed by pseudo-second-order kinetics and the molecular chemical interactions. At optimum PH (~7), the value of k_2 is 18 and 15 for DLX and LVX, respectively. The higher value of k_2 for DLX indicates the strong affinity of OGA-Pc-O-CMCS hydrogel for DLX in comparison with LVX. For both antibiotics, the kinetic data fitted well

Table 3. Constants and correlation coefficient of pseudo-first-order and pseudo-second-order kinetic models

Sample	pH	$Q_e^{(exp)}$ (mg/g)	Pseudo-first-order			Pseudo-second-order		
			R^2	$Q_e^{(cal)}$ (mg/g)	K_1 (min^{-1})	R^2	$Q_e^{(cal)}$ (mg/g)	K_2 (mg/g·min)×10^4
LVX	1	10.3	0.874	19.6	0.056	0.992	16.1	3.6
	7	24.5	0.982	24.1	0.047	0.993	29.4	15
	11	18.1	0.913	23.7	0.032	0.985		7.4
DLX	1	9	0.971	18.7	0.041	0.991	15.4	5.6
	7	26.7	0.954	24.8	0.044	0.986	32.1	18
	11	21.4	0.972	28.5	0.054	0.987	27.3	8.2

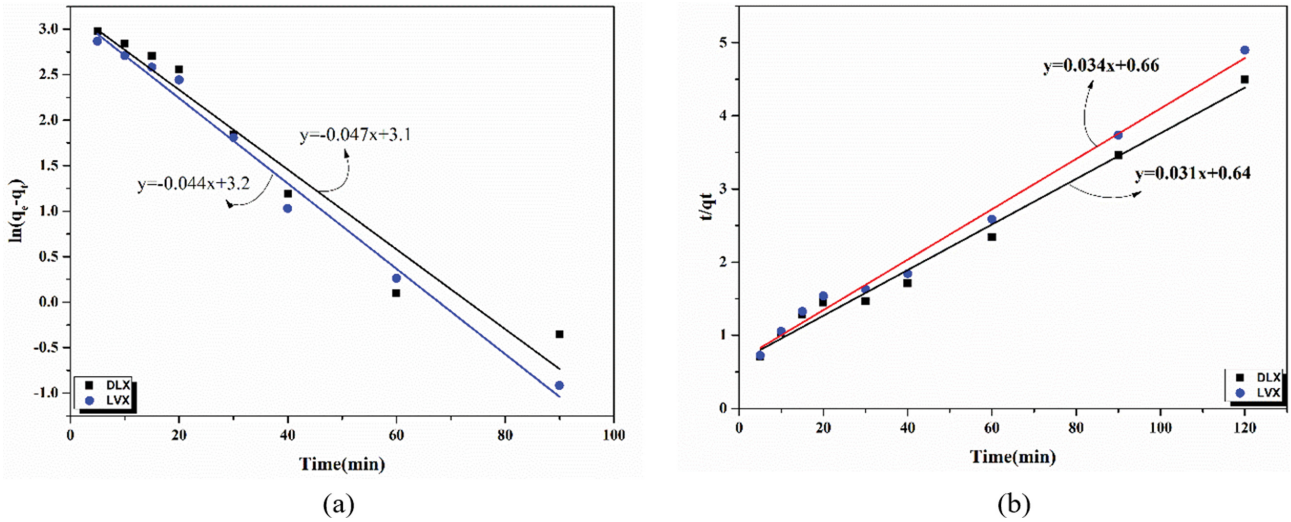

Fig. 12. The constants and correlation coefficient of (a) pseudo-first-order and (b) pseudo-second-order kinetic models.

Table 4. The values of ΔG^o, ΔS^o and ΔH^o for DLX and LVX absorption onto OGA-Pc-O-CMCS hydrogel

Temperature	ΔG^o		ΔS^o		ΔH^o (Kj/mol)	
	DLX	FLX	DLX	FLX	DLX	FLX
25	−2	−3.1				
35	−2.6	−3.8	57.7	58.1	15.2	16.8
45	−3.1	−4.6				

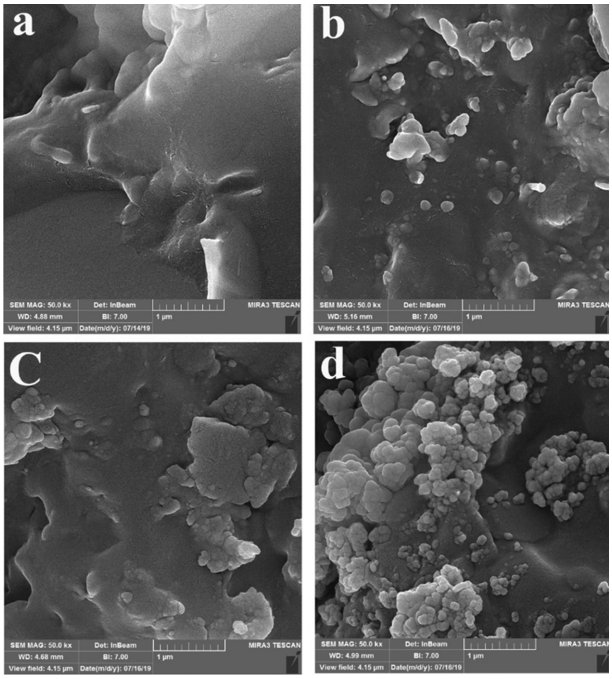

Fig. 13. FE-SEM micrograph of (a) OGA-cl-Pc-O-CMCS, (b) OGA-cl-Pc-O-CMCS+LVX, (c) OGA-cl-Pc-O-CMCS+DLX and (d) OGA-cl+Pc-O-CMCS+45% OGA.

to the pseudo-second-order kinetics with correlation coefficient of 0.99.

The values of ΔG^o, ΔS^o, and ΔH^o for both antibiotics are presented in Table 4. Negative values of ΔG^o for DLX and LVX indicate the spontaneous nature of the adsorption reaction. The higher negative value of ΔG^o at higher temperatures revealed that the adsorption was more conceivable at higher temperatures. The positive value of ΔH^o represented that the adsorption process was endothermic for both antibiotics.

5. Morphological Properties

The morphological characterization of the optimized hydrogel before and after antibiotics adsorption was visualized using FE-SEM as shown in Fig. 13(a)-(d). It can be seen that, before antibiotics adsorption, the structure of the beads was homogeneous, intact, and compact with a dense surface (Fig. 13(a)). After LVX or LDX adsorption, the crystalline layers of the antibiotics were formed within the hydrogel domain (as shown in Fig. 13(d)).

CONCLUSION

In the present work, an impressive method was extended for antibiotics removal from water by hydrogel. The prepared hydrogel consists of Pc/OCS cross-linked by gum arabic that is fabricated by a facile co-precipitation/crosslink technique. The adsorption data show that OGA-Pc-O-CMCS hydrogel was a proper adsorbent for the removal of antibiotics Delafloxacin (DLX) and Levofloxacin (LVX) from a water system. It was observed that the adsorption efficiency of DLX was more than LVX because of the q_m value, 171 mg/g for DLX and 200 mg/g for LVX. DLX represented better nucleophile in comparison with LVX; therefore, higher adsorption was taking place for DLX. The nucleophilicity distinction between the two antibiotics originated from different groups of flour and amine groups in DLX and LVX. Different nucleophilicity of the antibiotics led to different interactions with the OGA-Pc-O-CMCS hydrogel. The SIPs model fitted better to the data compared to the Langmuir and Freundlich models. The performance of the synthesized hydrogel indicates that this type of hydrogel system can be a desirable and efficient adsorbent for antibiotic absorption.

ACKNOWLEDGEMENT

The research is done at the Yasouj university and no funds have been used.

CONFLICT OF INTEREST

Conflict of interest the authors declare that they have no conflict of interest.

SUPPORTING INFORMATION

Additional information as noted in the text. This information is available via the Internet at http://www.springer.com/chemistry/journal/11814.

REFERENCES

1. V. M. Vaughn, S. M. Seelye, X. Q. Wang, W. L. Wiitala, M. A. Rubin and H. C. Prescott, *Inpatient and discharge fluoroquinolone prescribing in Veterans Affairs hospitals between 2014 and 2017*, presented at the Open Forum Infectious Diseases (2020).
2. M. Bilal, S. Mehmood, T. Rasheed and H. M. Iqbal, *Curr. Opin. Environ. Sci. Health*, **13**, 68 (2020).
3. E. Felis, J. Kalka, A. Sochacki, K. Kowalska, S. Bajkacz, M. Harnisz and E. Korzeniewska, *Eur. J. Pharmacol.*, **866**, 172813 (2020).
4. N. Benarab and F. F. Fangninou, *Int. J. Sci. Res. Publ. IJSRP*, **10** (2020).
5. K. M. Onesios, T. Y. Jim and E. J. Bouwer, *Biodegradation*, **20**(4), 441 (2009).
6. A. Anglada, A. Urtiaga and I. Ortiz, *J. Chem. Technol. Biotechnol.*, **84**(12), 1747 (2009).
7. D. Kanakaraju, B. D. Glass and M. Oelgemöller, *J. Environ. Manage.*, **219**, 189 (2018).
8. K. Li, X. Lu, Y. Zhang, K. Liu, Y. Huang and H. Liu, *Environ. Res.*, **185**, 109 (2020).
9. I. Ali, O. M. Alharbi, Z. A. ALOthman, A. M. Al-Mohaimeed and A. Alwarthan, *Environ. Res.*, **170**, 389 (2019).
10. S. Gu, X. Kang, L. Wang, E. Lichtfouse and C. Wang, *Environ. Chem. Lett.*, **17**(2), 629 (2019).
11. R. Baby, B. Saifullah and M. Z. Hussein, *Nanoscale Res. Lett.*, **14**(1), 1 (2019).
12. P. Samaddar, S. Kumar and K.-H. Kim, *Polym. Rev.*, **59**(3), 418 (2019).
13. S. Iftekhar, D. L. Ramasamy, V. Srivastava, M. B. Asif and M. Sillanpää, *Chemosphere*, **204**, 413 (2018).
14. N. S. Capanema, A. A. Mansur, H. S. Mansur, A. C. de Jesus, S. M. Carvalho, P. Chagas and L. C. de Oliveira, *Environ. Technol.*, **39**(22), 2856 (2018).
15. Z. Bao, C. Xian, Q. Yuan, G. Liu and J. Wu, *Adv. Healthc. Mater.*, **8**(17), 190 (2019).
16. M. Chen, Z. Ni, Y. Shen, G. Xiang and L. Xu, *Colloids Surf. A Physicochem. Eng.*, **602**, 125 (2020).
17. X. Liang, C. Ma, X. Yan, H. Zeng, D. J. McClements, X. Liu and F. Liu, *Food Hydrocoll.*, **102**, 105 (2020).
18. M. Amr, M. Counts, J. Kernan, A. Mallah, J. Mendenhall, B. Van Wie, N. Abu-Lail and B. A. Gozen, *Bioprinting*, **22**, 133 (2021).
19. M. Perini, D. Bertoldi, T. Nardin, S. Pianezze, G. Ferrari and R. Larcher, *Food Hydrocoll.*, **105**, 105 (2020).
20. A. Sudalai, A. Khenkin and R. Neumann, *Org. Biomol. Chem.*, **13**(15), 4374 (2015).
21. S. Manjunath and M. Kumar, *Chemosphere*, **262**, 127 (2021).
22. H. Gong, M. Liu, B. Zhang, D. Cui, C. Gao, B. Ni and J. Chen, *Int. J. Biol. Macromol.*, **49**(5), 1083 (2011).
23. G.-Q. Huang, L.-Y. Cheng, J.-X. Xiao and X.-N. Han, *Colloid Polym. Sci.*, **293**(2), 407 (2015).
24. A. Z. Tareq, M. S. Hussein and A. M. Mustafa, *Int. Res. J. Pure Appl.*, **12**(4), 1 (2016).
25. K. Gupta and F. H. Jabrail, *Carbohydr. Res.*, **341**(6), 744 (2006).
26. J. L. Drury and D. J. Mooney, *Biomaterials*, **24**(24), 4337 (2003).
27. M. Sarafrazi, M. Hamadanian and A. R. Ghasemi, *Mech. Mater.*, **138**, 103 (2019).
28. B. Sarker, D. G. Papageorgiou, R. Silva, T. Zehnder, F. Gul-E-Noor, M. Bertmer, J. Kaschta, K. Chrissafis, R. Detsch and A. R. Boccaccini, *J. Mater. Chem. B*, **2**(11), 1470 (2014).
29. J. Lach, *Water*, **11**(6), 1141 (2019).
30. B. E. Reed and M. R. Matsumoto, *Sep. Sci. Technol.*, **28**, 2179 (1993).
31. A. M. Carvajal-Bernal, F. Gomez-Granados, L. Giraldo and J. C. Moreno-Pirajan, *Eur. J. Chem.*, **8**(2), 112 (2017).
32. N. Tzabar and H. ter Brake, *Adsorption*, **22**(7), 901 (2016).
33. M. I. Mouzam, M. Dehghan, S. Asif, T. Sahuji and P. Chudiwal, *Saudi. Pharm. J.*, **19**(2), 85 (2011).

Supporting Information

Oxidized gum arabic cross-linked pectin/O-carboxymethyl chitosan: An antibiotic adsorbent hydrogel

Reza Darvishi*,†, Hajar Moghadas*, and Ali Moshkriz**

*Department of Gas and Petroleum, Yasouj University, Gachsaran, 75918-74831, Iran
**Department of Chemical Engineering, Faculty of Engineering, Arak University, Arak, 38156-8-8349, Iran
(*Received 28 June 2021 • Revised 13 November 2021 • Accepted 10 December 2021*)

Table S1. DOE matrix and results

Run	X_1 (Time)	X_2 (Temp)	X_3 (PH)	X_4 (OGA)	Y_1 (Swelling)	Y_2 (Crosslink Degree)
1	10	3	60	15	144.5	46.6
2	20	3	60	15	114.8	60.1
3	10	7	60	15	116	62.3
4	20	7	60	15	89.8	75.8
5	10	3	80	15	127	63.2
6	20	3	80	15	92.3	78.5
7	10	7	80	15	105	78.8
8	20	7	80	15	67.2	94.2
9	10	3	60	35	129.1	37.9
10	20	3	60	35	99.4	51.4
11	10	7	60	35	96.6	55
12	20	7	60	35	66.9	68.5
13	10	3	80	35	109.6	54.2
14	20	3	80	35	74.9	69.6
15	10	7	80	35	77.1	71.4
16	20	7	80	35	42.4	86.7
17	5	5	70	25	127	55.9
18	25	5	70	25	57.5	87.9
19	15	1	70	25	142.9	38.9
20	15	9	70	25	85.3	71.6
21	15	5	50	25	96	64.8
22	15	5	90	25	54	99.5
23	15	5	70	5	128.1	62.3
24	15	5	70	45	87.8	46
25	15	5	70	25	83.5	78
26	15	5	70	25	84.2	78.1
27	15	5	70	25	81	77
28	15	5	70	25	78.7	76
29	15	5	70	25	79.7	76.5
30	15	5	70	25	82.4	77.6

Table S2. ANOVA data for the two response-surface models

	Y_1 (Swelling)					Y_2 (Crosslink degree)				
Source	Sum of square	df	Mean square	F-value	Prob>F	Sum of square	df	Mean square	F-value	Prob>F
Model	19,814.628	14	1,415.33	676.83	<0.0001	6,821.07	14	487.22	1,410.19	<0.0001
X_1	6,540.60	1	6,540.60	3,127.81	<0.0001	1,342.51	1	1,342.51	3,885.70	<0.0001
X_2	4,982.40	1	4,982.40	2,382.66	<0.0001	1,612.12	1	1,612.12	4,666.05	<0.0001
X_3	2,513.30	1	2,513.30	1,201.90	<0.0001	1,811.34	1	1,811.34	5,242.67	<0.0001
X_4	2,424.06	1	2,424.06	1,159.22	0.9458	394.47	1	394.47	1,141.74	<0.0001
X_1X_2	0.0100	1	0.01	0.0048	0.0003	0.0006	1	0.0006	0.0018	0.9666
X_1X_3	44.22	1	44.22	21.15	0.9458	3.33	1	3.33	9.64	0.0072
X_1X_4	0.0100	1	0.01	0.0048	0.2860	0.0006	1	0.0006	0.0018	0.9666
X_2X_3	2.56	1	2.56	1.22	0.0001	0.0006	1	0.0006	0.0018	0.9666
X_2X_4	54.02	1	54.02	25.83	0.0250	2.03	1	2.03	5.88	0.0284
X_3X_4	12.56	1	12.96	6.20	0.0001	0.0506	1	0.05	0.1465	0.7072
X_1^2	247.89	1	247.89	118.54	0.0250	37.67	1	37.67	109.02	<0.0001
X_2^2	1,967.17	1	1,967.17	940.73	<0.0001	780.50	1	780.50	2,259.03	<0.0001
X_3^2	46.80	1	46.80	22.38	<0.0001	53.04	1	53.04	153.52	<0.0001
X_4^2	1,317.73	1	1,317.73	630.16	0.0003	863.04	1	863.04	2,497.95	<0.0001
Lack of fit	21.05	10	2.11	1.02	<0.0001	3.28	1	0.32	0.8663	0.6070

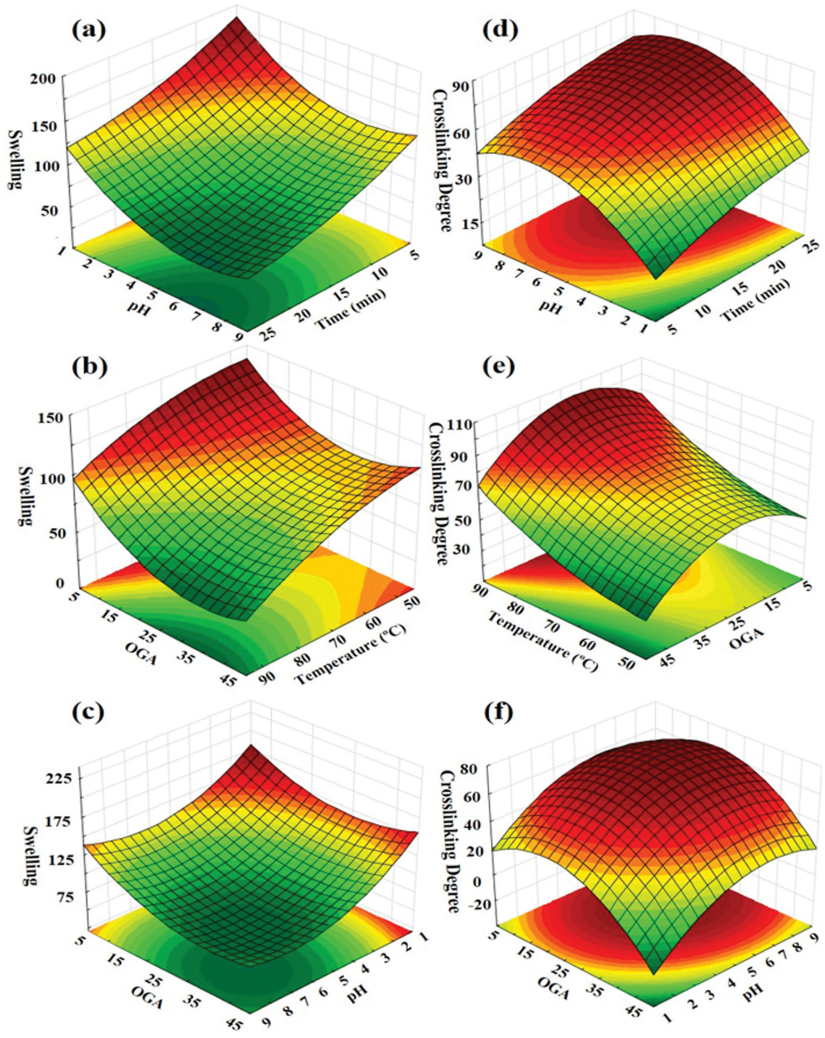

Fig. S1. Response surfaces plots for different variables at optimum conditions.